04

Three-electrode gas-discharge system — plasma-chemical microreactor

© L.M. Portsel, Yu.A. Astrov, A.N. Lodygin, E.V. Beregulin

Ioffe Institute,
194021 St. Petersburg, Russia
e-mail: leonid.portsel@mail.ioffe.ru

Received December 18, 2024
Revised March 18, 2025
Accepted April 07, 2025

The study investigates suitability of three-electrode semiconductor-gas-discharge system as a microreactor for plasma-chemical treatment of a semiconductor material surface. The system is composed of two discharge gaps separated with a metal grid that serves as a common electrode. A self-sustained low-energy DC Townsend discharge is formed in the first gap. Charged particles of the discharge pass through the grid meshes and move in the electric field of the second gap. Sample surface treatment takes place in the second gap due to the interaction between the charged particle flux and semiconductor. Experiments were performed in a three-electrode system filled with argon. GaAs is used as a sample. Modification of surface properties was determined using spectroscopic ellipsometry. It is shown that semiconductor irradiation by argon ions Ar^+ leads to removal of an oxide layer from the surface and formation of a 5−20 nm modified near-surface layer. The layer is composed of a mixture of crystalline and amorphous GaAs.

Keywords: gas dischare, GaAs semiconductor, surface property modification, ellipsomety.

DOI: 10.61011/TP.2025.10.62091.462-24

Introduction

Plasma-chemical treatment techniques are used in various fields of science and technology from food disinfection [1] to plasma treatment of graphene [2]. Promising techniques include methods using low intensities of plasma-chemical impact on the treated object. One of the methods for modifying material surface properties is semiconductor treatment with a low-energy DC Townsend discharge. This discharge occurs in a semiconductor-gas-discharge system (SGD) [3,4]. This system is a thin gas-discharge gap, one of the electrodes of which is made from a high-resistance photo-sensitive semiconductor material — semi-insulating (SI) GaAs.

When a relatively high voltage of approximately 300−500 V is applied to the electrodes of the gas-discharge gap, a low-energy DC Townsend discharge with spatially-uniform current distribution occurs in a SGD system. At typical values of gas-discharge gap lengths $d_1 \approx 50-200\,\mu$m and ion concentration on the discharge cathode of $\sim 0.02-2.0 \cdot 10^9\,\mathrm{cm}^{-3}$, electric field distortion induced by a spatial ion charge is insignificant. Therefore, at all current densities used in the experiments, gas-discharge sustaining voltage remained constant.

Various types of instabilities can develop in the gas discharge and, in systems with metal electrodes, lead to oscillations or current filaments [5,6]. In a gas discharge system with a high-resistance electrode, growth of current fluctuations and development of instabilities are suppressed. This is due to local voltage drop across the distributed electrode resistance and occurrence of negative feedback between current and voltage in the gap. This „stabilized“ discharge at small interelectrode distances has all attributes of a low-energy DC Townsend discharge: volume burning and independence of discharge sustaining voltage on current. Discharge exists in a wide range of gas pressures $p \approx 10 - 500$ hPa and current densities $J \approx 10 - 500\,\mu\mathrm{A/cm}^2$. In this case, a semiconductor electrode must have a sufficiently high resistivity $\rho > 10^6\,\Omega\cdot$cm. At lower electrodes resistances, instabilities in the form of oscillations or spatiotemporal structures occur in the SGD system [7].

The application of SGD microdischarge devices for formation of oxide layers with a thickness of several nanometers on the surface of semiconductor compounds such as GaAs, InAs and InAlAs was reported in [8–10]. The processed sample was used as one of the SGD system electrodes. For experiments, polarity of voltage applied to the system electrodes was chosen such that the sample served as anode of the discharge gap and semiconductor surface oxidation occurred due to the action of electrons and Townsend discharge products. In the case of reverse polarity [8], the sample served as a discharge gap cathode and semiconductor surface was irradiated by gas discharge ions. Interaction between ions and the semiconductor caused structural modifications of the material surface layer.

The requirement for high resistivity of the sample processed in the SGD system limits the applicability of this technique. In [11], a three-electrode microreactor design was proposed to provide spatially homogeneous treatment of samples in the case of their high conductivity. Such system consists of two discharge gaps that have a common electrode in the form of a metal grid. A self-sustained Townsend discharge with a stable spatially homogeneous

state is realized in the first gap. This region of the device excites a non-self-sustained discharge in the second gap, which is maintained by the flux of charged particles passing through the grid. Sample treatment in this microreactor section is performed by means of gas discharge products. As a result, stable device operation doesn't depend on the resistance of the treated sample, thus, offering obvious advantages compared with the above-mentioned two-electrode SGD device. Note that such three-electrode planar systems were used before to study a photographic process in AgBr [12] and an infrared (IR) image converter [13].

This study investigates the possibility of using the three-electrode system proposed in [11] for semiconductor material treatment with gas-discharge ions. The aim of this work is also to study the neutralization of low-kinetic-energy ions the semiconductor surface and to determine the composition of the modified surface layer formed as a result of this process.

The experiments were performed in a three-electrode system with Townsend discharge excitation in Ar at gas pressures of $p = 20 - 200$ hPa. The features of discharge burning with grid cathode and ion flux formation in the microreactor region, where a semiconductor was processed, were investigated. Properties of the sample's near-surface layer were studied by spectroscopic ellipsometry.

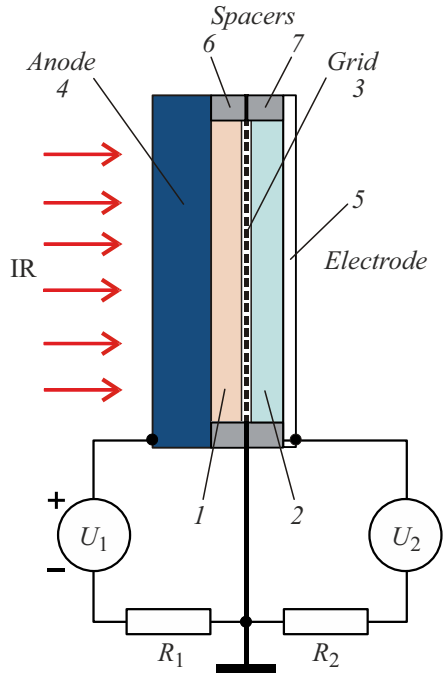

Figure 1. Three-electrode SGD system diagram: *1* — gas-discharge gap, in which the Townsend discharge was excited, *2* — second gap, *3* — grid, *4* — semiconductor electrode, *5* — second gap electrode, *6*, *7* — dielectric spacers, U_1 — gas discharge voltage source. U_2 — voltage source, IR — IR flux.

1. Experimental technique and measurement results

The three-electrode system diagram is shown in Figure 1. Gap *1* was formed by a hole in dielectric spacer *6* placed between semiconductor electrode *4* and metal grid *3*. The electrode was made of photosensitive semi-insulating (SI) GaAs. Spectral sensitivity range of such material is $\lambda = 0.8 - 1.7\,\mu$m. The external surface of electrode has a transparent electric contact formed by vacuum thermal spraying of metal (Ni). The GaAs electrode was illuminated by an IR source, which allowed the electrode resistance to be controlled by varying the light intensity.

Gap *2* was formed by a hole in dielectric spacer *7* placed between the grid and electrode *5*. A glass plate with conducting SnO_2 coating was used as an electrode. Resistance of this electrode was $\sim 100\,\Omega$. Experiments for semiconductor treatment with gas-discharge ions used a GaAs sample with low resistivity as an electrode.

Electrode *3* was made of a woven metal grid with a spatial period of 15 l/mm and the square mesh center-to-center distance $a = 66\,\mu$m. Wire diameter d was $18\,\mu$m. The size of free space in a mesh cell — „aperture" —, were $\sim 48 \times 48\,\mu$m.

The device was powered by two voltage supply sources with polarities shown in Figure 1. Resistors R_1 and R_2 served to measure the discharge current in gap *1* and the charged particle current in gap *2*, respectively.

The three-electrode SGD system was placed in a closed chamber with optical windows to illuminate the electrode and to observe the spatial homogeneity of discharge combustion. Gas discharge image was recorded by the PIEPER CCD camera. The incandescent tungsten lamp was used as the light source. The chamber was filled with Ar at the gas pressure $p = 20 - 200$ hPa. Positive voltage $+U_1$ was applied between electrode *4* and grid *3*. At U_1 exceeding the gas breakdown voltage, a self-sustained Townsend discharge with spatially homogeneous current density distribution J_1 is formed in the first gap. Discharge current was determined by gas pressure, applied voltage U_1 and electrode *4* resistance that depended on the semiconductor illumination intensity. The system was fed from the High Voltage Power Supplies PS300 Stanford Research Systems DC power supply. To maintain constant J_1, the power supply was set to the constant current mode. Gas discharge current density in gap *1* was maintained at $J_1 = 50\,\mu$A/cm^2 almost in all experiments. In case of measurements carried out with other value of J_1, a necessary explanation will be provided in the text as appropriate. In addition, all experiments within this study were carried out on the SGD system with the following gas-discharge gap lengths: the first gap - $d_1 = 200\,\mu$m, and the second gap - $d_2 = 120\,\mu$m. Areas of the first and second gaps were $S_1 = 2$ cm^2 and $S_2 = 1$ cm^2, respectively.

Polarity of voltage U_1 applied to the first gap electrodes in the experiments was chosen such that the grid served as the gas discharge cathode and current in the grid region was caused by the ion flux. A part of charged particles passed

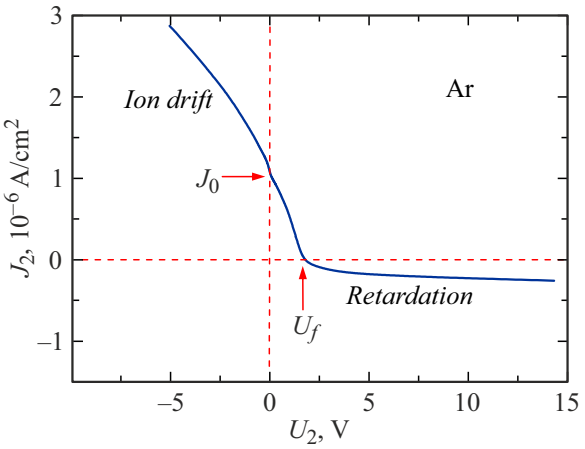

Figure 2. Dependence of current density in gap (2) on voltage. Gas pressure $p = 50$ hPa. Discharge current density $J_1 = 50\,\mu$A/cm^2. See the text for explanations.

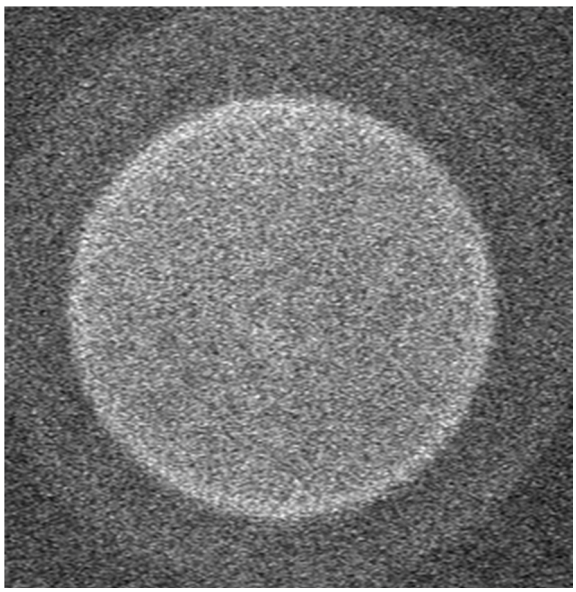

Figure 3. Image of discharge glow in the first gap. Diameter of the dark ring corresponds to the diameter of hole in spacer (*6*) that forms the gas-discharge region. Bright disk is the image of discharge that is seen through the grid and the second gap.

through the grid meshes and entered gap *2*. In this case, an electric current J_2 appeared in the circuit — electrode *5* — power supply — resistor R_2. The current was defined as voltage drop across R_2. Voltage was measured using the KEITHLEY 2000 voltmeter with high input resistance > 10 GΩ. The magnitude and polarity of U_2 defined the form of volt-ampere characteristic (VAC) of gap *2*.

Figure 2 shows the typical VAC for gap *2*, the electrode of which was a glass plate with conducting coating. As can be seen from the figure, at $U_2 = 0$ in gap *2*, there was current J_0 caused by ions injected from the discharge in gap *1*. J_0 is marked on the diagram with a horizontal arrow.

Figure 3 shows the image of discharge luminescence in the first gap at $U_2 = 0$. The bright image corresponds to the discharge glow seen through the grid and is limited by the hole size in dielectric spacer *7*. Diameter of the hole in spacer *6* that forms the gas-discharge region is larger than the second gap area diameter. A part of the discharge image is seen through the grid and spacer *7* made of mica. Therefore the image of this region is darker. The discharge has volume burning with spatially homogeneous current distribution. Ions injected from the discharge into the second gap also have spatially homogeneous distribution.

When the voltage U_2 applied to electrode *5* is negative, ions in the second gap are accelerated (ion drift), leading to an increase in the ion current J_2. This mode was used for operation of the three-electrode SGD system as a microreactor for semiconductor material processing. When the ion flux interacts with semiconductor in the second gap, sample surface properties are modified. Spatially homogeneous ion flux distribution ensures uniform modification of the surface properties.

When U_2 is positive, ions that have passed through the grid are retarded (Figure 2). J_2 decreases, and at some value of U_2 the current becomes equal to zero. As U_2 further increases, the sign of current is reversed and a negative VAC branch is observed. Current in this region is probably related to electrons, that are formed as a result of photoionization of gas atoms by radiation from the discharge in the first gap.

The shape of VAC (Figure 2) resembles the Langmuir probe VAC. Similarly, U_f, at which J_2 becomes equal to zero may be defined as the floating potential. This value is marked on the diagram with a vertical arrow.

As it turned out from the experiments, J_2 with $U_2 = 0$ depended on R_2. To study this specific feature of system operation, experiments were performed without using the second gap power supply. For this, R_2 was connected directly between grid *3* at zero potential and electrode *5*. The glass plate was used as the electrode. Voltage drop across R_2 corresponded to electrode *5* potential.

Figure 4, *a* shows a log-log scale dependence $U(R_2)$ of electrode *5* potential on R_2. Figure 4, *b* shows the dependence of injected ion current density $J_2(R_2) = U(R_2)/R_2$. The data is shown for three pressures $p = 20$, 50 and 150 hPa. The length of gas-discharge gap *1* was $d_1 = 200\,\mu$m. At such system parameters, values $p \cdot d_1$ corresponded to the minimum and right-hand branch of the Paschen curve.

When load resistances are lower than $10^5\,\Omega$, linear dependence $U(R_2)$ is observed, and as the resistance grows further, the voltage across electrode *5* reaches its limit value U_0. When load resistances are low, J_2 remains almost constant and decreases with increasing R_2.

Such dependence of U and J_2 on R_2 may be explained by considering the equivalent circuit diagram consisting of power supply U_0 with internal resistance R_{D2} and load resistance R_2. The voltage U across the load resistance in

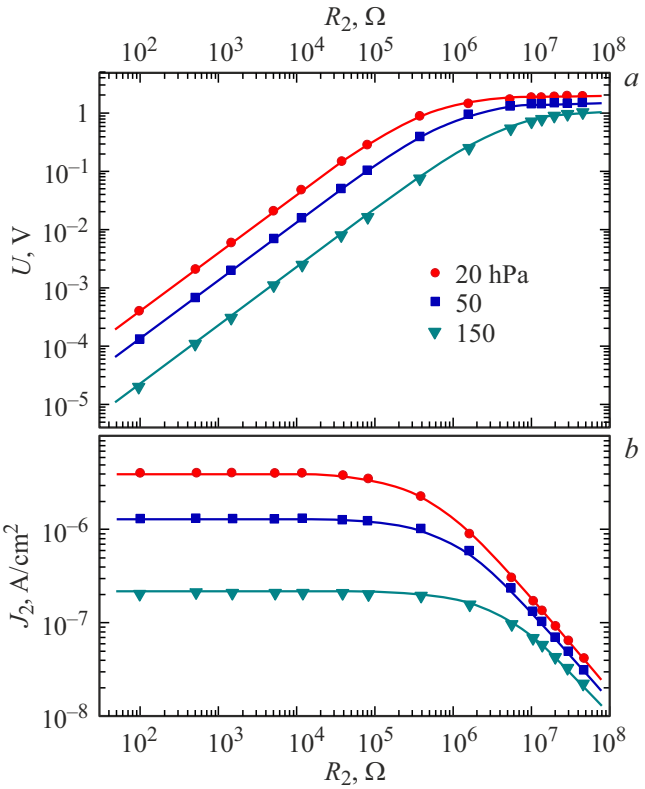

Figure 4. *a* — dependence of U across electrode (*5*) on R_2; *b* — injected ion current density in the second gap J_2. Symbols correspond to values measured at $p = 20$, 50 and 150 hPa. Solid curves — calculation using equation (1), U_0 and R_{D2} were used as adjustable parameters.

this case is equal to

$$U = \frac{U_0 R_2}{R_{D2} + R_2}. \qquad (1)$$

Current $J = U/R_2$ in such circuit depends on the ratio of the internal resistance of power supply R_{D2} to load resistance R_2. Thus, when the load resistance is much lower than R_{D2}, the current weakly depends on R_2 and is equal to $J \approx U_0/R_{D2}$. As can be seen from the diagram, such current is maintained within the load resistance range up to $R_2 \approx 10^5 - 10^6\,\Omega$. As the load resistance increases at $R_2 > R_{D2}$, the current suddenly decreases and tends to $J = U_0/R_2$.

Solid lines in Figure 4 show $U(R_2)$ and $J_2(R_2)$ calculated using equation (1). U_0 and R_{D2} were used as adjustable parameters. Table 1 shows U_0, R_{D2} and J_0 obtained from experimental data processing for $p = 20 - 150$ hPa.

VAC of the second gap (Figure 2) was measured at $R_2 = 12\,\text{k}\Omega$. Thus, J_0 marked with arrow in Figure 2 corresponds to constant J_2 and can serve as one of the system state parameters.

The second gap current at $U_2 = 0$ is related to drift-diffusion movement of ions in a weak electric field, which is caused by potential distortion in grid meshes. As mentioned above, the free space (aperture) dimensions in the mesh were $\sim 48 \times 48\,\mu$m. $d_2 = 120\,\mu$m is comparable with the grid mesh dimension. With such system parameter ratio, strong distortion of potential in grid meshes is possible and electric field of the discharge can penetrate the second gap [14,15]. The averaged potential in *2* may be associated with voltage supply U_0 of equivalent circuit, and R_{D2} may be related with the second gap resistance that is determined by the ion flux.

Application of positive U_2 to electrode *5* when measuring VAC (Figure 2) induces additional electric field in the second gap that retards ions and causes current reduction. $J_2 = 0$ is reached in case when the electric field U_f/d_2 compensates the field caused by the potential distortion in grid meshes. Thus, U_0 and U_f have a closely related physical meaning. Figure 5 shows the dependence of U_0 on the gas pressure. The data was plotted using a log-log scale. Increase in pressure leads to a decrease in electrode *5* potential. The plot also shows U_f measured at the same pressures. As can be seen, U_0 and U_f have approximately the same values at relatively low pressures and differ at $p > 70$ hPa.

Dependence of current density on gas pressure $J_{R=100}(p)$ measured at $R_2 = 100\,\Omega$ and $U_2 = 0$ (Figure 4, *b*) is shown in the inset in Figure 5. An increase in the gas pressure leads to a decrease in current density. An increase in U_0 and $J_{R=100}$ with pressure growth can be probably explained by the grid's electrical transparency variation.

Figure 6, *a* shows VAC of the second gap measured at negative U_2 and $p = 50$, 75 and 100 hPa. With such voltage polarity, ions injected from the discharge in the first gap are accelerated in the second gap electric field. At $U_2 \approx 0 - 10$ V, current nonlinearity is observed, and at higher voltages, current dependence becomes almost linear. Ion concentration N_{ion} may be calculated from the

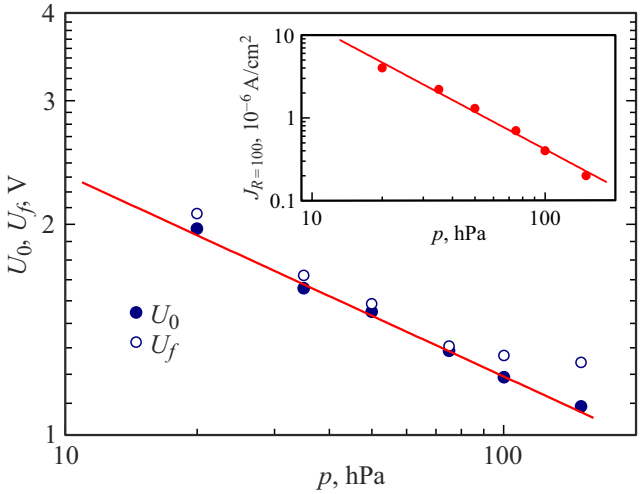

Figure 5. Dependence of U_0 and U_f on gas pressure. The inset shows the dependence of $J_{R=100}$ on pressure measured at $R_2 = 100\,\Omega$ and $U_2 = 0$.

Table 1. U_0, R_{D2} and $J_2(R_2 = 100\,\Omega)$ measured for $p = 20 - 150$ hPa

d_2, μm	Data	p, hPa					
		150	100	75	50	35	20
120	U_0, V	1.1	1.2	1.3	1.5	1.62	2
	R_{D2}, Ω	$5 \cdot 10^6$	$3.2 \cdot 10^6$	$2.0 \cdot 10^6$	$1.2 \cdot 10^6$	$7 \cdot 10^5$	$5.0 \cdot 10^5$
	$J_2(100)$, μA/cm^2	0.2	0.4	0.7	1.3	2.2	4.0

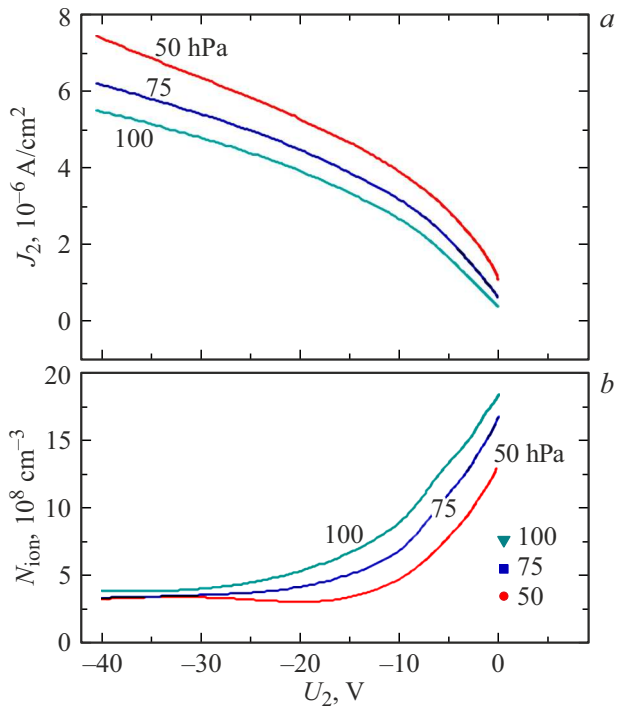

Figure 6. *a* — dependence of the current density J_2 on the second gap voltage U_2 at the gas pressures $p = 50$, 75 and 100 hPa; *b* — ion concentration in the second gap depending on U_2 determined from VAC for various gas pressures. Symbols show ion concentrations at the discharge cathode in the first gap $N_{cathode}$.

differential resistance of the second gap:

$$N_{ion}(U_2) = \frac{\Delta J_2 d_2}{\Delta U_2 q \mu(p)}, \qquad (2)$$

where ΔJ_2 and ΔU_2 are the current density and voltage variations, respectively, q is the electron charge, $\mu(p) = 1444/p\,\text{cm}^2 \cdot \text{V}^{-1} \cdot \text{s}^{-1}$ (p is measured in mmHg) — ion mobility [16].

$N_{ion}(U_2)$ calculated using equation (2) for $p = 50$, 75 and 100 hPa are shown in Figure 6, *b* with solid lines. Symbols correspond to ion concentrations at the discharge cathode in the first gap — grid *3*. Concentrations were calculated for the given gas pressures and $J_1 = 50\,\mu$A/cm^2 as $N_{cathode} = J_1 d_1/(q\mu U_S)$. The discharge sustaining voltage was $U_S = 207$, 227, 250 V for the corresponding gas pressures.

At zero and relatively low voltage U_2, ion concentration in gap *2* N_{ion}, as shown in the figure, is higher than the ion concentration at the cathode $N_{cathode}$. The flux of ions injected from the discharge is larger than the flux of ions drifting in the low field of the second gap. As the field increased, the ion flux speed increases, and at $U_2 > 10$ V, N_{ion} becomes lower than at the cathode. In such conditions, N_{ion} in the second gap is limited mainly by the discharge current J_1 and grid's electrical transparency. VAC approaches the linear dependence. VAC nonlinearities at low voltages are thus related to the excess ion concentration in the second gap compared with the ion concentration at grid *3* — discharge cathode in the first gap $N_{cathode}$.

2. Example of semiconductor treatment with ions

Experiments for semiconductor surface treatment with gas-discharge ions used a *n*-GaAs sample with the resistivity $\rho \approx 1\,\Omega$·cm. Original GaAs wafers 28 mm in diameter and 0.56 mm in thickness were polished mechanically. Then, the damaged 50 μm surface layer was removed from the sample by chemical-mechanical polishing using 5–8 % NaOCl solution in water. After the appropriate treatment, the GaAs wafer was placed into the microreactor (Figure 1).

Irradiation was performed at the gas-discharge gap length $d_1 = 200\,\mu$m, $d_2 = 120\,\mu$m at Ar pressure $p = 50$ hPa. Gas discharge current density was set to $J_1 = 200\,\mu$A/cm^2. J_2 was determined by U_2, and the irradiation dose $Q = J_2 \cdot t$ was defined by the current density and process time t.

Structural changes in the semiconductor surface layer were evaluated using spectroscopic ellipsometry (SE). Measurements were performed before and after ion treatment of the GaAs sample surface using the SEMILAB SE2000 ellipsometer at the angle of light incidence $\varphi_0 = 70°$ within a photon energy range of $E = 1.5 - 5.0$ eV. Light polarization variation after reflection from the sample surface was defined as the complex number ρ equal to the ratio of reflection coefficients with polarization parallel R_S and perpendicular R_P to the incidence plane:

$$\rho = \frac{R_P}{R_S} = \tan\Psi e^{i\Delta}, \qquad (3)$$

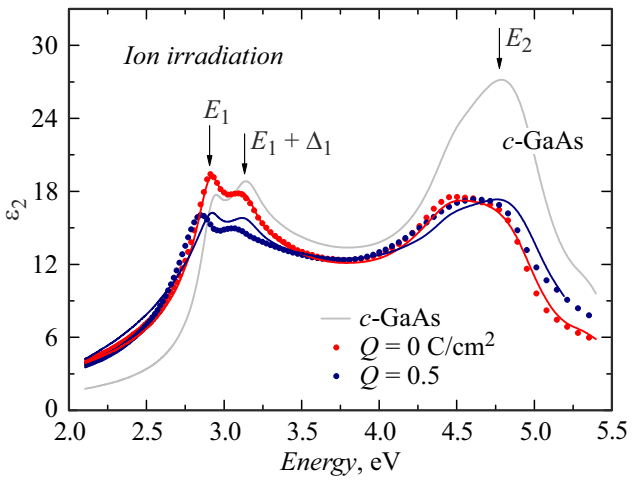

Figure 7. Spectrum of the imaginary part of pseudo-dielectric function. Symbols correspond to the experimental values of $\varepsilon_2(E)$ obtained from the SE data for the GaAs samples with different Ar^+ irradiation doses:—Q = 0 and 0.5 C/cm^2. Solid lines are the calculated dependences in the EMA model of the surface layer. The PD function layer of the crystalline *c*-GaAs is also shown on the curve.

where Ψ and Δ are polarization angles experimentally measured by the ellipsometer.

Surface layer structure and thickness were obtained by comparing the SE data with the model calculation. A three-layer model consisting of a GaAs wafer, surface layer and vacuum (air) was used. Dielectric function of the layer corresponded to the chosen material or was determined using the Bruggeman effective medium approximation (EMA). A real surface layer in this approximation was replaced by a layer consisting of different materials and having the effective dielectric function of a medium [17]. Model parameters corresponding to the layer thickness and composition were varied to minimize the error between the experimental and calculated spectral dependences of the polarization angles Ψ, Δ. Ellipsometer software was used.

The complex pseudo-dielectric function (PD) $\varepsilon = \varepsilon_1 + i \cdot \varepsilon_2$ was calculated using a model of light reflection from a homogeneous semi-infinite medium [18]. This function is directly related to the semiconductor electronic structure and determines the optical properties of the surface.

Figure 7 shows the dependences of the imaginary part $\varepsilon_2(E)$ of the PD function on the photon energy calculated for various Ar^+ irradiation doses. The data corresponds to a sample with untreated surface and an ion-irradiated sample with $Q = 0.5$ C/cm^2. The plot also shows $\varepsilon_2(E)$ of the PD function of the crystalline *c*-GaAs. The spectrum contains peaks at E_1, $E_1 + \Delta_1$ ($h\nu = 2.91$ and 3.14 eV) and E_2 (4.77 eV) that correspond to interband transitions at critical points of the GaAs crystal structure [19,20].

Spectral dependence of the imaginary part of PD for the sample with untreated surface differs from PD of the crystalline *c*-GaAs. The main changes are observed in the $\sim 4.5 - 5$ eV spectral region. Light penetration depth at such photon energies is at its minimum, values of ε_2 PD in this spectral region are most sensitive to the surface condition. XPS (X-ray photoelectron spectroscopy) measurements [6] showed that the surface of GaAs samples contained an oxide layer — Ga_2O_3 and As_2O_3. Ga_2O_3 is the most stable compound. Therefore, the SE calculations used a layer model with the dielectric function of this material. Layer thickness obtained by comparing the calculation with the experiment was 3 nm. Solid line in the plot show the calculated dependence $\varepsilon_2(E)$.

Ar^+ irradiation of the sample surface leads to a decrease in the spectrum maxima amplitude and a slight shift of doublet energies E_1, $E_1 + \Delta_1$ into a lower energy region. Identical changes in the dielectric function spectra of GaAs samples were observed in [8,21,22] when the semiconductor surface was treated by gas discharge ions and during ion implantation. The authors of these works attributed the change in the optical properties of semiconductor surface to the formation of a damaged crystal structure region in the material. Accumulation of structural defects in the lattice gives rise to amorphous layers on the semiconductor surface. Dielectric function of layers with damaged structure is generally determined on the assumption that the material is a physical mixture of crystalline and amorphous GaAs, and the effective medium approximation (EMA) is used.

XPS measurements of the chemical composition profile of samples performed in [8] didn't find any change in the semiconductor material composition and any oxides resulting from N_2^+ irradiation of the semiconductor. The quoted study assumed that the modified layer consisted of a *c*-GaAs, *a*-GaAs and Void mixture. The Void material has a dielectric function of vacuum and inclusion of this component in the layer physically means either surface roughness or material porosity.

Solid lines in the figure show the dependences of the imaginary part of PD ε_2 obtained by fitting the experimental SE and calculated data in the model of the modified *c*-GaAs, *a*-GaAs, Void layer. Material percentage and layer thickness for different doses $Q = 0.023 - 0.5$ C/cm^2 are shown in Table 2. The table also shows the thickness of the Ga_2O_3 layer on the untreated semiconductor surface.

Figure 7 shows that the GaAs model with natural oxide layer adequately describes the optical properties of the untreated surface. Unfortunately, for the Ar^+ irradiated sample, such coincidence of the calculated and experimental $\varepsilon_2(E)$ was not observed. The authors of [22] noted that the EMA model is not always able to correctly describe the dielectric function spectrum in transition from a crystalline to amorphous material. The best result may be achieved in an approximation where the dielectric function is represented in the form of superposition of harmonic oscillators. Nevertheless, the analysis of GaAs surface irradiation effect was limited to the EMA model that allowed the damaged layer thickness to be determined.

Table 2. Parameters of the modified GaAs layer model with different Ar^+ irradiation doses obtained by comparing the experimental and calculated SE data

Dose, C/cm^2	Modified GaAs layer				Thickness, nm
	Ga_2O_3, %	*c*-GaAs, %	*a*-GaAs, %	Void, %	
0	100				3.2
0.025	92	–	8	–	2.9
0.056		67	12	21	6.88
0.1		67	20	13	12.6
0.3		67	20	13	14.5
0.5		63	27	10	15.7

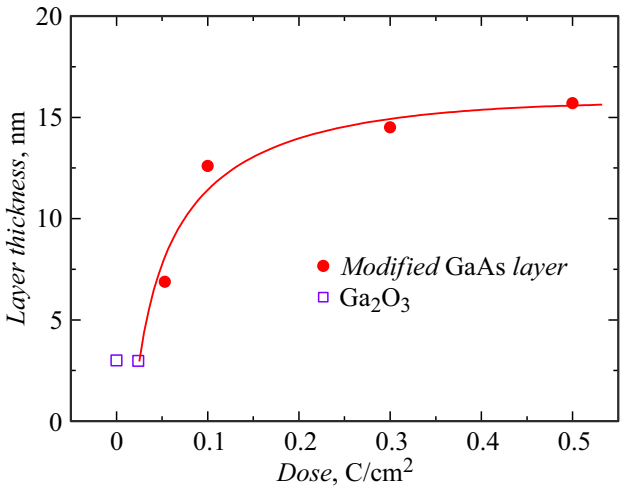

Figure 8. Dependence of the damaged layer thickness on the Ar^+ irradiation dose of GaAs.

Figure 8 shows the damaged layer thickness depending on the ion irradiation dose $Q = J_2 \cdot t$ C/cm^2. As mentioned above, the untreated GaAs surface has a ~ 3 nm Ga_2O_3 layer. Ar^+ irradiation of the semiconductor with a low dose $Q = 0.025$ C/cm^2 leads to insignificant changes in the SE data compare with the untreated surface. Satisfactory coincidence of the theoretical and experimental dependences Ψ, Δ was obtained by including a small amount of amorphous *a*-GaAs together with Ga_2O_3 into the modified layer model (Table 2). As the irradiation dose increases, the oxide layer disappears and a damaged layer, composition of which is shown in Table 2, is formed on the surface. The layer composition slightly varies as the irradiation dose increases. Dependence of the layer thickness on the dose is nonlinear.

Conclusion

The study investigates injection of positively charged ions from a self-sustained Townsend discharge that modify the properties of semiconductor materials when interacting with their surface. The effect is studied in a planar three-electrode structure with a metal grid used as the common electrode. Stability of the spatially homogeneous state of gas-discharge processes in the device is provided by the fact that one of the electrodes in the self-sustained discharge region is made from a semiconductor with high resistivity. Low space charge density in the gaps makes it possible to interpret the observed phenomena using simple concepts of gas discharge physics. From an experimental standpoint, the studied structure is also interesting in that it allows one to investigate the processes of positive ion injection into a gas medium as well as to study the stationary states of non-self-sustained discharges.

The three-electrode SGD system was used for experimental Ar ion treatment of a GaAs semiconductor sample with different irradiation doses $Q = 0.025 - 0.5$ C/cm^2. Sample resistivity was $\sim 1\,\Omega$·cm. It is shown that the interaction between Ar^+ and GaAs surface leads to oxide removal and formation of a material layer with a damaged structure consisting of a crystalline and amorphous GaAs mixture. In the experiments, the average kinetic energy of the ions only slightly exceeded the thermal energy of the gas atoms. The observed of structural changes in the near-surface region of the crystal is possibly related to the mechanism of charged particle neutralization on the semiconductor surface. Ion neutralization takes place as a result of the Auger process where a semiconductor valence band electron tunnels into the ion ground state [23]. Energy released during the ion neutralization is transferred to the semiconductor subsystem and may induce structural defects.

The low kinetic energy ion injection technique discussed in the work is supposed to be used, with an appropriate composition, for plasma-chemical treatment of condensed media, both dielectric and conducting.

Acknowledgments

The authors appreciate the assistance provided by V.A.Tolmachev and V.O.Bolshakov in conducting ellipsometric measurements.

Conflict of interest

The authors declare no conflict of interest.

References

[1] C. Pignata, D. D'Angelo, E. Fea, G. Gilli. J. Appl. Microbiol., **122**, 1438 (2017). DOI: 10.1111/jam.13412
[2] A. Dey, A. Chroneos, N.St.J. Braithwaite, R.P. Gandhiraman, S. Krishnamurthy. Appl. Phys. Rev., **3**, 021301 (2016).
[3] Yu.A. Astrov, V.V. Egorov, Sh.S. Kasymov, V.M. Murugov, L.G. Paritsky, S.M. Ryvkin, Yu.N. Sheremetiev. Kvantovaya elektronika, **4** (8), 1681 (1977) (in Russian).
[4] V.M. Marchenko, H.-G. Purwins, L.M. Portsel, Yu.A. Astrov. *Semiconductor-Gas-Discharge Device for Fast Imaging in the Infrared, Physics, Engineering and Applications* (Shaker Verlag, Aachen, 2016)
[5] Z.Lj. Petrović, A.V. Phelps. Phys. Rev. E, **27**, 2806, 2825 (1993).
E.L. Gurevich, Yu.P. Raizer, H.G. Purvins. ZhTF, **76** (2), 36 (2006) (in Russian).
[7] L.M. Portsel, A.N. Lodygin, Yu.A. Astrov. J. Phys. D: Appl. Phys., **42**, 235208 (2009).
[8] E.L. Gurevich, S. Kittel, R. Hergenröder, Yu.A. Astrov, L.M. Portsel, A.N. Lodygin, V.A. Tolmachev, A.V. Ankudinov. J. Phys. D: Appl. Phys., **43**, 275302 (2010). DOI: 10.1088/0022-3727/43/27/275302
[9] M.S. Aksenov, A.Yu. Kokhanovskii, P.A. Polovodov, S.F. Devyatova, V.A. Golyashov, A.S. Kozhukhov, I.P. Prosvirin, S.E. Khandarkhaeva, A.K. Gutakovskii, N.A. Valisheva, O.E. Tereshchenko. Appl. Phys. Lett., **107**, 173501 (2015).
[10] M.S. Aksenov, A.K. Gutakovskii, I.P. Prosvirin, D.V. Dmitriev, A.A. Nedomolkina, N.A. Valisheva. Mater. Sci. Semicond. Process., **102**, 104611 (2019).
[11] Yu.A. Astrov, A.N. Lodygin, L.M. Portsel, A.A. Sitnikova. J. Appl. Phys., **124**, 103303 (2018). DOI: 10.1063/1.5042487
[12] Yu.A. Astrov, V. Zhelev, J. Malinowski, S.M. Ryvkin. Phys. Status Solidi (a), **61**, K127 (1980).
[13] T. Yuldashev, Z. Khaidarov, Sh.S. Kasymov. Uspekhi prikladnoi fiziki (in Russian), **4** (6), 580 (2016).
[14] F.H. Read, N.J. Bowring, P.D. Bullivant, R.R.A. Ward. Rev. Sci. Instrum., **69**, 2000 (1998). DOI: 10.1063/1.1148888
[15] P.D. Goldan, F.L.J. Yadlowsky, E.C. Whipple Jr. J. Geophys. Res., **78**, 2907 (1973).
[16] A.L. Ward. Phys. Rev., **112** (6), 1852 (1958).
[17] D.A.G. Bruggeman. Ann. Phys. (Leipzig), **24**, 636 (1936).
[18] R.M.A. Azzam, N.M. Bashara. *Ellipsometry and Polarized Light* (Amsterdam, North-Holland, 1977)
[19] P. Lautenschlager, M. Garriga, S. Logothetidis, M. Cardona. Phys. Rev. B, **35**, 9174 (1987).
[20] S. Ozaki, S. Adachi. J. Appl. Phys., **78**, 3380 (1995).
[21] E. Schubert, N. Razek, F. Frost, A. Schindler, B. Rauschenbach. J. Appl. Phys., **97**, 023511 (2005).
[22] M. Erman, J.B. Theeten, P. Chambon. J. Appl. Phys., **56**, 2664 (1984).
[23] H.D. Hagstrum. Phys. Rev., **122**, 83 (1961).

Translated by E.Ilinskaya

Translated by E.Ilinskaya